Adaptive Square-Root Cubature Kalman Filter Based Low Cost UAV Positioning in Dark and GPS-denied Environments

Beiya Yang, *Member, IEEE*, Erfu Yang, *Senior Member, IEEE*, Haobin Shi, Leijian Yu, *Member, IEEE* and Cong Niu, *Member, IEEE*

***Abstract*—Routine inspection inside the water tank, pressure vessel, penstocks and boiler which present dark and global positioning system (GPS) denied environment always plays an important role for the safety storage and transportation. The conventional inspection conducted by the skilled workers is highly expensive, time consuming and may cause the safety and heath problem. Nowadays, the emerging unmanned aerial vehicle (UAV) based techniques make it possible to replace human to do the periodical inspection in these environments. However, how to obtain the reliable, high accuracy and precise position information of the UAV becomes a challenging issue, as the GPS is unable to provide the accurate position information in these environments. In order to resolve this problem, an adaptive square-root cubature Kalman filter (ASRCKF) based low cost UAV positioning system is designed. Through the combination of the inertial measurement unit (IMU), ultra-wideband (UWB), the cubature rule, the adaptively estimated noise model and weighting factors, the potential degradation and oscillation for the system performance which caused by the linearisation process, the variation of the measurement noise and the manually adjusted noise model are solved. Finally, the 0.081m median localisation error, 0.172m 95^{th} percentile localisation error and 0.045m average standard deviation (STD) can be attained, which can support the UAV to achieve the autonomous inspection in dark and GPS-denied environments.**

***Index Terms*—Unmanned aerial vehicle (UAV), ultra-wideband (UWB), autonomous inspection, GPS-denied environments, adaptive Kalman filter (AKF), adaptive square-root cubature Kalman filter (ASRCKF).**

I. Introduction

In the industrial practices, the periodical inspection for the storage or shipping containers such as the water tank, the pressure vessel, penstocks and boiler known as dark and global positioning system (GPS) denied environments, to inspect if the cracks and corrosion exist is indispensable [1]–[9]. Currently, the inspection inside these environments is carried out by the well trained workers, which is inefficient, laborious, high cost and has the potential safety and heath problem. Nowadays, with the development of the unmanned aerial vehicle (UAV) based technique, it becomes possible to replace human with the UAV to do the periodical inspection in these environments. However, considering the unavailability of the satellite signal, the acquisition of the accurate and precise UAV position information has been turned into the challenging issue to be resolved [10]–[15].

Currently, the researches have already been carried out for the high accuracy and precision UAV localisation in dark and GPS-denied environments to achieve the detailed inspection. Within these, the vision based techniques, especially for the visual odometry (VO) are the extensively used localisation techniques for UAV, on account of the high accuracy and implementation simplicity characteristics [16], [17]. However, the performance of the vision based techniques is greatly limited by the illumination condition and the texture within the operational environment, which is not suitable for the applications in dark environment. To tackle this issue, through the coupling of a nonlinear model predictive control (NMPC) with a visual processing scheme, Kanellakis et al. [18] achieved the autonomous navigation of the micro aerial vehicle (MAV) in the challenging dark environment. Instead of the positioning of the MAV, the vision based approach is only utilised to regulate the heading direction of the MAV. However, it is still difficult for the detailed inspection with the proposed system, considering the requirement of the precise position information. Similarly, to limit the performance influence led by the changing illumination and the light noises, a UAV and ground guide vehicle cooperation system was proposed in [19]. With the visual fiducial equipped on the ground guide vehicle and the dual-source images based visual positioning approach, the relative localisation of the UAV can be achieved for the under bridge inspection. Yet, the performance of their system is greatly influenced and limited, considering the difficulty to deploy the ground guide vehicle for the focused application scenarios, and the performance influence of vision based techniques in completely dark environment. From different perspectives, a MAV based vessel inspection system was designed and implemented in [1]. For the accurate

This work was supported in part by the UK Net Zero Technology Centre under Grant AI-P-028, the Royal Society under Grant IEC-NSFC-211434. Beiya Yang is now supported in part by the National Key Research and Development Program of China under Grant SQ2023YFF0900037, the Fundamental Research Funds for the Central Universities under Grant No. D5000230340 and the Key Research and Development Program of Shaanxi under Grant 2023-GHZD-42.

Beiya Yang and Haobin Shi are within the School of Computer Science, Northwestern Polytechnical University, Xi'an 710072, China. The work belongs to Beiya Yang's PhD project, which has been conducted and finished in UK. Prof. Haobin Shi provides significant help on the revision of this paper.

Erfu Yang is within the Department of Design, Manufacturing and Engineering Management, University of Strathclyde, Glasgow G1 1XJ, UK.

Leijian Yu is within the Centre for Additive Manufacturing, Faculty of Engineering, University of Nottingham, Nottingham NG8 1BB, UK.

Cong Niu is within the Innova NanoJet Technology Limited, RD, Glasgow, UK.

The corresponding authors are Dr. Erfu Yang (UK, erfu.yang@strath.ac.uk) and Prof. Haobin Shi (China, shihaobin@nwpu.edu.cn).

UAV positioning under different circumstances, three different sensor suites were offered. The UAV positioning for the first sensor suit mostly relies on a forward looking camera, which means that the performance is limited by the illumination condition of the operational environment. To restrict the impact coming from the illumination condition or the texture within the operational environment, the laser scanner is utilised as the main localisation component for the second sensor suit. However, the increased cost, size and energy consumption of the positioning components all make it impossible for the low cost applications on the small UAV. Meanwhile, the positioning performance of the system is also restricted by the "canyoning" effect. To provide a reliable and robust positioning performance, the combination of the first two sensor suits is made. Nevertheless, the weight, size, cost and energy consumption of the system are still not taken into account. Similarly, authors in [20]–[23] all utilised the laser scanner or the light detection and ranging (LiDAR) based localisation system for UAV positioning to overcome the low illumination condition. Nevertheless, the aforementioned issue for the LiDAR and laser scanner based system still has the great impact on the applications with MAV. Moreover, with the built-in inertial measurement unit (IMU) on the current UAV platform, the IMU based positioning has also attracted lots of attentions on the UAV positioning. However, the error accumulation issue makes it impossible to utilise the single IMU for high performance positioning. Thus, it often serves as part of the sensor fusion approach for UAV positioning. Most recently, the commercial UAV named Elios 2 developed by Flyability attracts lots of attention, due to the ability for the inspection inside the constrained space such as the sewers, mines and oil and gas vessels. However, the skilled engineer is required to manually control the Elios 2 which will certainly elevate the potential crash risk and still laborious. Thus, a low cost localisation technique which is capable for the precise, accurate and reliable localisation of the UAV is still pressingly required to support the stable flight in these environments. In the last couple of years, the researches on the ultra-wideband (UWB) based UAV positioning technique have been conducted due to the high accuracy (up to centimetre), low cost, light weight, high position update rate, no performance impact regardless of the illumination conditions and robustness to against the multi-path effect characteristics [24], [25]. These all make it to be the potential candidate for the focused applications. Nevertheless, the performance oscillation led by the unreasonable values and variation of the measurement noise within the ranging information for the pure UWB based technique still greatly limits the applications on UAV.

To overcome these limitations, the Kalman filter (KF) based localisation algorithms which integrated the IMU and the UWB have been investigated and extensively utilised for UAV positioning. In [26], to achieve the low cost UAV positioning, the extended Kalman filter (EKF) was exploited to do the sensor fusion of IMU and UWB. The additional measurement calibration and outlier detection methods have been proposed to resist the performance influence from the unreasonable values. Similarly, authors in [27] presented a sensor fusion based localisation system through the EKF algorithm, which successfully achieved the 80Hz 3D positioning of the MAV swarm with the utilisation of the IMU and UWB. The same research has also been carried out by Strohmeier et al. [28], but differently, excluding the UAV position, the angular rate was introduced to estimate the precise attitude information. Whereas, with the utilisation of the first order Taylor expansion for the EKF, the neglected high order terms still limit its performance. To remedy this, the advanced KF algorithms were proposed. Instead of linearising the observation matrix, the system state can be approximated by the sampling points for the unscented Kalman filter (UKF). According to the UAV flight test results in [29], the accuracy of the system is significantly increased by 70% in comparison with the pure UWB based system. Yet, considering the operational environments in this article, it is difficult to collect the UAV after crash, the priority for the positioning system is to avoid any position lost of the UAV. Thus, the increased probability for filtering divergence and computational complexity of the UKF based approaches restrict the applications in the focused scenarios [30]. For further improvement, the cubature Kalman filter (CKF) and square-root cubature Kalman filter (SRCKF) were proposed [31]. Leveraging the spherical-radial cubature rule, the approximation for the state posterior mean and covariance can be achieved [32]. Compared with the EKF and UKF based approaches, the potential performance degradation led by the linearisation can be eliminated with slightly increased computational complexity and stable filtering performance which is suitable for the focused UAV applications.

On the other hand, for all the KF based sensor fusion approaches, the process and measurement noise covariance matrices known as the $\boldsymbol{Q}$ and $\boldsymbol{R}$ matrices have the significantly impact on the system positioning performance [33]–[35]. The unsuitable noise covariance in the estimation process can even lead to the positioning failure [36], [37]. Thus, how to acquire the appropriate noise covariance matrices should also be considered, especially for the focused applications, since it is hard to manually adjust these in dark and GPS-denied environments. Due to the existing characteristics for the adaptive Kalman filter (AKF) based approach, including the implementation simplicity and low computational complexity, it becomes to one of the ideal candidates to remedy this issue.

In our previous work [38], an adaptive extended Kalman filter (AEKF) based sensor fusion algorithm was presented to overcome the UAV localisation performance influence caused by the unsuitable noise covariance matrices in the same environments. The adaptive estimation was successfully achieved through the recorded offline data and the measurements. Meanwhile, two additional weighting factors were added in the algorithm to further improve the performance and stability of the algorithm for the UAV applications in the same environments. Nevertheless, the linearisation error led by the neglected high order terms still has the great impact on its performance under certain circumstances. Moreover, the negative estimation of the measurement noise covariance matrix may exist, which will lead to the positioning failure. In the previous algorithm, if a negative estimation is detected, the offline data will be directly utilised as the noise covariance matrices in this estimation round. Obviously, the adaptive ability of the algorithm will

be decreased. Under such circumstance, in order to overcome all these issues, a new approach is still desired for the performance improvement.

In order to address all the above issues, in this paper, an adaptive square-root cubature Kalman filter (ASRCKF) based low cost UAV localisation system is proposed to support the autonomous inspection inside dark and GPS-denied environments. Accordingly, the main contributions of this paper are highlighted below:

1) An ASRCKF based sensor fusion algorithm is proposed for the reliable, high accuracy and high precision UAV positioning in dark and GPS-denied environments. In contrast with the existing KF approaches, the performance degradation, oscillation and potential positioning failure caused by the linearisation process, the unsuitable and potential negative estimation of the noise covariance matrices can be significantly reduced and eliminated. Furthermore, to avoid the potential positioning failure and limit the huge variation of the estimated noise covariance matrices, the additional dynamic weighting factors are added to keep a more reliable UAV positioning performance.
2) Low cost IMU and UWB based sensor fusion UAV positioning algorithm and system are designed to replace humans for the detailed autonomous inspection inside dark and GPS-denied environments.
3) Comprehensive simulations, experiments and actual flight tests with the inspection task in the laboratory environment have been conducted to validate the algorithm and system performance. According to the results, the presented system and algorithm are able to attain a high level localisation performance of the UAV with the 0.081m median localisation error, 0.172m 95^{th} percentile localisation error and 0.045m average standard deviation (STD) and achieve the autonomous inspection in dark and GPS-denied environments.

This article is organised as follows. Firstly, the structure for the proposed system is introduced in Section II. Followed by, the description for the proposed ASRCKF based IMU and UWB sensor fusion localisation algorithm is given in Section III. In order to do the comprehensive verification of the proposed ASRCKF algorithm and UAV positioning system, the analysis and discussion for the simulation and experiment results are presented in Section IV. Finally, the conclusion for the whole article is made in Section V.

II. System diagram

For the purpose of the low cost UAV positioning to support the autonomous inspection inside dark and GPS-denied environments, the following system as shown in Fig. 1 is designed. Clearly, the system consists of six modules including the central module (ground station), UAV module, IMU module, UWB based localisation module, recording module and reference module, according to the function of each module. As seen from the system diagram, the central module known as a Linux laptop is responsible for all the calculations and control related functions. The UAV module known as a commercial low cost quadcopter named Bebop2 is responsible for the autonomous inspection. The IMU module, which is integrated within the UWB tag node (the UWB sensor node to be located), is leveraged to get the acceleration and attitude information for the position and attitude control of the UAV. The UWB based localisation module including the tag node (mounted on the UAV) and the anchor nodes (the position information is known) is responsible for providing the ranging information for UAV position estimation. For the purpose of providing the high quality images and videos for the detailed inspection, an additional recording module the commercial Insta 360 Go2 is utilised in the system. This is under the consideration of the size, price, weight, image and video quality (2560x1440, 50fps), and the exiting FlowState stabilisation function which is significant for the UAV based applications. Finally, the reference module known as the V120:Trio designed by OptiTrack is responsible for providing the ground truth of the UAV position information during the experiments. The total price for the system is around £1200, including the UAV (Bebop2), one IMU, UWB tag and UWB listener node, four UWB anchor nodes and the Insta 360 Go2. It needs to note that the reference module is only responsible to get the ground truth, therefore, the price for this module is not included.

III. IMU and UWB based UAV positioning

Accordingly, considering the issues for the pure UWB and the traditional KF sensor fusion techniques, including the degradation and oscillation for the localisation performance led by the linearisation of the observation matrix, the variation of the measurement noise, the unreasonable values within the measured ranging information and the potential filtering divergence results from the unsuitable noise covariance matrices, an ASRCKF based sensor fusion algorithm is presented and introduced in this section to overcome all these issues.

A. Mathematical model

With the existing kinematic model of the UAV [39], the matrix form for the motion equation can be derived

$$\hat{\boldsymbol{\gamma}}_{k/k-1} = \boldsymbol{F}_k \boldsymbol{\gamma}_{k-1} + \boldsymbol{B}_k \boldsymbol{a}^L_{k-1}, \tag{1}$$

where, $\boldsymbol{\gamma} = [x, v_x, y, v_y, z, v_z]^T$ denotes the state vector composed by the UAV position and velocity in three directions, $\boldsymbol{a}^L = [a^L_x, a^L_y, a^L_z]^T$ is supposed as the acceleration in local navigation coordinate system in three directions measured by the IMU, k is the round number of the estimation process, $\boldsymbol{F}$ and $\boldsymbol{B}$ represent the state transition matrix and the control matrix respectively, which can be written as

$$\boldsymbol{F} = \begin{bmatrix} 1 & \Delta T & 0 & 0 & 0 & 0 \\ 0 & 1 & 0 & 0 & 0 & 0 \\ 0 & 0 & 1 & \Delta T & 0 & 0 \\ 0 & 0 & 0 & 1 & 0 & 0 \\ 0 & 0 & 0 & 0 & 1 & \Delta T \\ 0 & 0 & 0 & 0 & 0 & 1 \end{bmatrix}, \tag{2}$$

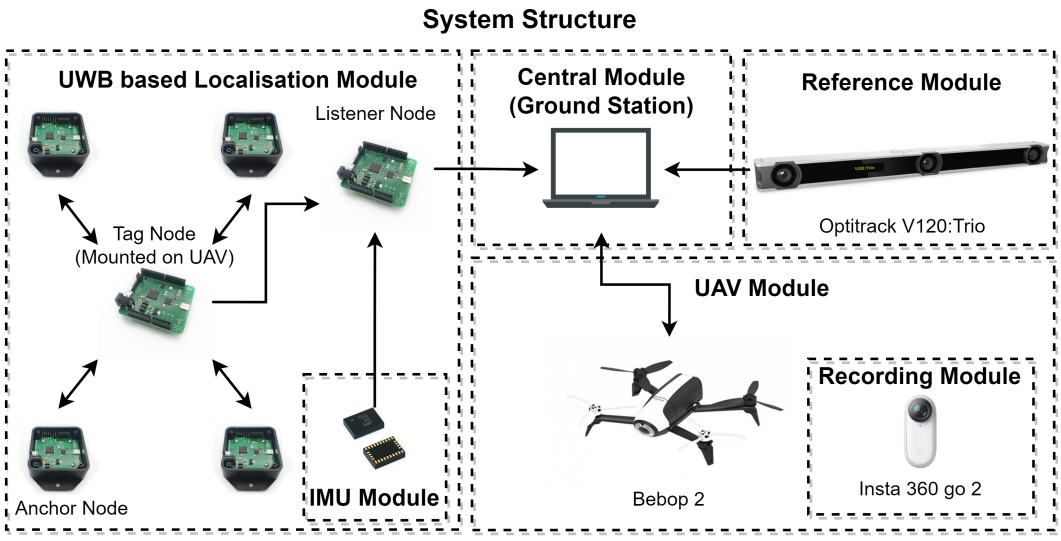

Fig. 1. System structure.

$$\boldsymbol{B} = \begin{bmatrix} \frac{\Delta T^2}{2} & 0 & 0 \\ \Delta T & 0 & 0 \\ 0 & \frac{\Delta T^2}{2} & 0 \\ 0 & \Delta T & 0 \\ 0 & 0 & \frac{\Delta T^2}{2} \\ 0 & 0 & \Delta T \end{bmatrix}, \tag{3}$$

ΔT is the time interval.

With the measured ranging information between the UWB sensor nodes, the correction for the predicted state information can be made as follows

$$\boldsymbol{Z}_k = \boldsymbol{H}_k \hat{\boldsymbol{\gamma}}_{k/k-1} + \boldsymbol{\omega}_k, \tag{4}$$

where, $\boldsymbol{Z} = [d_1, d_2, ..., d_n]^T$ represents the measurement matrix, d_n denotes the ranging information between the tag node and anchor node n, $\boldsymbol{\omega} \sim N(\boldsymbol{0}, \boldsymbol{R})$ is assumed as the measurement noise for the ranging information measured by the UWB nodes, $\boldsymbol{R}$ denotes the measurement noise covariance matrix and $\boldsymbol{H}$ is supposed as the observation matrix. Obviously, the ranging information cannot be linearly represented by the predicted state vector $\hat{\boldsymbol{\gamma}}_{k/k-1}$. Thus, the first order Taylor expansion is exploited by the EKF based approach to linearise the observation matrix $\boldsymbol{H}$. However, this is at the expense of neglecting the high order terms, which are linked to the positioning performance of the algorithm and system.

B. SRCKF algorithm

To remedy the performance influence from the linearisation of the observation matrix, the cubature rule is utilised by SRCKF to approximate the state posterior mean and covariance [31], [32]. Here, the estimation process of the SRCKF is given as follows.

1) State prediction: Firstly, the cubature points are evaluated through the state vector $\boldsymbol{\gamma}_{k-1}$ and $\boldsymbol{S}_{k-1}$ from the $k-1$ round.

$$\boldsymbol{\gamma}_{i,k-1} = \boldsymbol{S}_{k-1}\boldsymbol{\xi}_i + \boldsymbol{\gamma}_{k-1}, i = 1, 2, ..., 2m, \tag{5}$$

where, m represents the number of the state variables to be estimated in the state vector, $\boldsymbol{S}_{k-1}$ denotes the square root of the covariance matrix $\boldsymbol{P}_{k-1}$ which can be calculated by the Cholesky decomposition

$$\boldsymbol{P}_{k-1} = \boldsymbol{S}_{k-1}\boldsymbol{S}_{k-1}^T, \tag{6}$$

$\boldsymbol{\xi}_i$ can be represented as

$$\boldsymbol{\xi}_i = \begin{cases} \sqrt{m}\boldsymbol{I}_{m,i}, i = 1, 2..., m \\ -\sqrt{m}\boldsymbol{I}_{m,i-m}, i = m+1, m+2, ..., 2m \end{cases}, \tag{7}$$

$\boldsymbol{I}_{m,i}$ is supposed as the ith column of the $m \times m$ identity matrix.

Accordingly, the propagated cubature points can be calculated through (1) and (5) and represented as

$$\boldsymbol{\gamma}^*_{i,k/k-1} = \boldsymbol{F}_k\boldsymbol{\gamma}_{i,k-1} + \boldsymbol{B}_k\boldsymbol{a}^L_{k-1}, i = 1, 2, ..., 2m. \tag{8}$$

Then, the predicted state vector and the square root of the covariance matrix can be derived as

$$\hat{\boldsymbol{\gamma}}_{k/k-1} = \frac{1}{2m}\sum_{i=1}^{2m}\boldsymbol{\gamma}^*_{i,k/k-1}, \tag{9}$$

$$\boldsymbol{S}_{k/k-1} = Tria([\boldsymbol{\Gamma}^*_{k/k-1}, \boldsymbol{S}_{Q,k-1}]), \tag{10}$$

where, Tria$(\cdot)$ denotes the QR decomposition, $\boldsymbol{S}_Q$ is supposed as the square root of the process noise covariance matrix $\boldsymbol{Q}$, $\boldsymbol{\Gamma}^*_{k/k-1}$ can be represented as

$$\begin{aligned} \boldsymbol{\Gamma}^*_{k/k-1} = &\frac{1}{\sqrt{2m}}[\boldsymbol{\gamma}^*_{1,k/k-1} - \hat{\boldsymbol{\gamma}}_{k/k-1}, \boldsymbol{\gamma}^*_{2,k/k-1} - \hat{\boldsymbol{\gamma}}_{k/k-1}, \\ &..., \boldsymbol{\gamma}^*_{2m,k/k-1} - \hat{\boldsymbol{\gamma}}_{k/k-1}] \end{aligned}. \tag{11}$$

2) Correction process: During the correction process for the SRCKF algorithm, firstly, the cubature points can be calculated through the predicted state vector and the square root of the covariance matrix from the prediction process and represented as

$$\boldsymbol{\gamma}_{i,k/k-1} = \boldsymbol{S}_{k/k-1}\boldsymbol{\xi}_i + \hat{\boldsymbol{\gamma}}_{k/k-1}, i = 1, 2, ..., 2m. \tag{12}$$

Followed by, the propagated cubature points can be derived through the calculated cubature points

$$\boldsymbol{Z}_{i,k/k-1} = h(k, \boldsymbol{\gamma}_{i,k/k-1}), i = 1, 2, ..., 2m, \tag{13}$$

where, h(·) is supposed as the observation function.

Then, the predicted measurement matrix can be expressed as

$$\hat{\boldsymbol{Z}}_{k/k-1} = \frac{1}{2m}\sum_{i=1}^{2m} \boldsymbol{Z}_{i,k/k-1}. \tag{14}$$

Throughout these, the square root of the innovation covariance matrix $\boldsymbol{S}_{ZZ,k/k-1}$ and the cross covariance matrix $\boldsymbol{S}_{\gamma Z,k/k-1}$ can be calculated as follows

$$\boldsymbol{S}_{ZZ,k/k-1} = Tria([\boldsymbol{\zeta}_{k/k-1}, \boldsymbol{S}_{R,k}]), \tag{15}$$

$$\boldsymbol{S}_{\gamma Z,k/k-1} = \boldsymbol{\Gamma}_{k/k-1}\boldsymbol{\zeta}^T_{k/k-1}, \tag{16}$$

where, $\boldsymbol{S}_R$ is assumed as the square root of the measurement noise covariance matrix $\boldsymbol{R}$, $\boldsymbol{\zeta}_{k/k-1}$ can be calculated by the propagated cubature points and the predicted measurement matrix

$$\begin{aligned}\boldsymbol{\zeta}_{k/k-1} =& \frac{1}{\sqrt{2m}}[\boldsymbol{Z}_{1,k/k-1} - \hat{\boldsymbol{Z}}_{k/k-1}, \boldsymbol{Z}_{2,k/k-1} - \hat{\boldsymbol{Z}}_{k/k-1},\\ & ..., \boldsymbol{Z}_{2m,k/k-1} - \hat{\boldsymbol{Z}}_{k/k-1}]\end{aligned}, \tag{17}$$

$\boldsymbol{\Gamma}_{k/k-1}$ can be represented as

$$\begin{aligned}\boldsymbol{\Gamma}_{k/k-1} =& \frac{1}{\sqrt{2m}}[\boldsymbol{\gamma}_{1,k/k-1} - \hat{\boldsymbol{\gamma}}_{k/k-1}, \boldsymbol{\gamma}_{2,k/k-1} - \hat{\boldsymbol{\gamma}}_{k/k-1},\\ & ..., \boldsymbol{\gamma}_{2m,k/k-1} - \hat{\boldsymbol{\gamma}}_{k/k-1}]\end{aligned}. \tag{18}$$

Finally, the Kalman gain $\boldsymbol{K}_{k,gain}$, corrected state vector $\hat{\boldsymbol{\gamma}}_k$ and the square root of the covariance matrix $\hat{\boldsymbol{S}}_k$ can be calculated and estimated as

$$\boldsymbol{K}_{k,gain} = (\boldsymbol{S}_{\gamma Z,k/k-1}/\boldsymbol{S}^T_{ZZ,k/k-1})/\boldsymbol{S}_{ZZ,k/k-1}, \tag{19}$$

$$\hat{\boldsymbol{\gamma}}_k = \hat{\boldsymbol{\gamma}}_{k/k-1} + \boldsymbol{K}_{k,gain}(\boldsymbol{Z}_k - \hat{\boldsymbol{Z}}_{k/k-1}), \tag{20}$$

$$\hat{\boldsymbol{S}}_k = Tria([\boldsymbol{\Gamma}_{k/k-1} - \boldsymbol{K}_{k,gain}\boldsymbol{\zeta}_{k/k-1}, \boldsymbol{K}_{k,gain}\boldsymbol{S}_{R,k}]). \tag{21}$$

C. ASRCKF algorithm

Apparently from the SRCKF algorithm, the potential performance degradation and oscillation results from the linearisation process can be limited. However, owing to the variation of the process and measurement noise model, when with the manually adjusted and constant $\boldsymbol{Q}$ and $\boldsymbol{R}$ matrices for the SRCKF, the performance degradation or even the positioning failure may appear [36]. Furthermore, the difficulty to manually adjust the noise covariance matrices in dark and GPS-denied environments should also be taken into account. Therefore, to overcome this, the ASRCKF algorithm is investigated and proposed in this subsection.

1) $\boldsymbol{Q}$ and $\boldsymbol{R}$ matrices estimation: Firstly, the estimation of the $\boldsymbol{R}$ matrix is discussed. Traditionally, it can be estimated through the innovation sequence calculated through the difference between the predicted measurement matrix from (14) and the measurement matrix $\boldsymbol{Z}_k$ in the current round [34]. Nevertheless, the negative estimation may exist, which will directly lead to the filtering divergence. To remedy this issue, inspired by the approach in [40], the measurement filtering residual $\boldsymbol{Z}'_k$ is calculated and exploited to estimate the measurement noise covariance matrix $\boldsymbol{R}$ to prevent the negative estimation issue.

With the corrected state vector $\hat{\boldsymbol{\gamma}}_k$ in (20) and the measurement matrix $\boldsymbol{Z}_k$ in the current round, the measurement filtering residual can be calculated and represented as

$$\boldsymbol{Z}'_k = \boldsymbol{Z}_k - h(k, \hat{\boldsymbol{\gamma}}_k). \tag{22}$$

Then, the $\boldsymbol{R}$ matrix in the current round can be obtained

$$\boldsymbol{R}_k = \hat{\boldsymbol{Q}}_{\boldsymbol{Z}'_k} + \hat{\boldsymbol{Z}}_{k/k-1}\hat{\boldsymbol{Z}}^T_{k/k-1}, \tag{23}$$

where, $\hat{\boldsymbol{Q}}_{\boldsymbol{Z}'_k}$ represents the residual covariance matrix which is calculated by the residual $\boldsymbol{Z}'_k$ from M rounds,

$$\hat{\boldsymbol{Q}}_{\boldsymbol{Z}'_k} = \frac{1}{M}\sum_{i=k-M+1}^{k} \boldsymbol{Z}'_i\boldsymbol{Z}'^T_i, \tag{24}$$

in which M denotes the size of the window. In the estimation process, if a smaller M is utilised, it means that the adaptive ability of the algorithm can be increased to catch up the changes in the current estimation process. But it is at the expense of the stability of the algorithm. On the other hand, larger M means the estimation of the residual covariance matrix will become stable and smooth, however, the adaptive ability will be greatly reduced and the computational complexity will be increased.

Through the mathematical model of the sensor fusion approach, it can be observed that the process noise $\boldsymbol{\eta}$ coming from the bias and measurement noise of the acceleration information can be expressed as

$$\boldsymbol{\eta}_{k-1} = \hat{\boldsymbol{\gamma}}_k - \hat{\boldsymbol{\gamma}}_{k/k-1}, \tag{25}$$

where,

$$\hat{\boldsymbol{\gamma}}_k - \hat{\boldsymbol{\gamma}}_{k/k-1} = \boldsymbol{K}_{k,gain}(\boldsymbol{Z}_k - \hat{\boldsymbol{Z}}_{k/k-1}). \tag{26}$$

Accordingly, the $\boldsymbol{Q}$ matrix can be obtained

$$\boldsymbol{Q}_{k-1} = \boldsymbol{K}_{k,gain}\hat{\boldsymbol{C}}_{\boldsymbol{Z}''_k}\boldsymbol{K}^T_{k,gain}, \tag{27}$$

where, $\hat{\boldsymbol{C}}_{\boldsymbol{Z}''_k}$ represents the innovation covariance matrix

$$\hat{\boldsymbol{C}}_{\boldsymbol{Z}''_k} = \frac{1}{M}\sum_{i=k-M+1}^{k} \boldsymbol{Z}''_i\boldsymbol{Z}''^T_i, \tag{28}$$

in which $\boldsymbol{Z}''_i$ denotes the innovation sequence in i round can be calculated through

$$\boldsymbol{Z}''_i = \boldsymbol{Z}_i - \hat{\boldsymbol{Z}}_{i/i-1}. \tag{29}$$

Obviously, the system is able to catch up the noise changes for performance improvement together with the aforementioned calculated $\boldsymbol{Q}$ and $\boldsymbol{R}$ matrices. Nevertheless, the huge

variation of these matrices in the actual process may lead to the instability of the filter and even cause the positioning failure. This is unacceptable for the focused applications. Thus, an additional approach is still required to avoid the potential filtering divergence and positioning failure.

2) Additional weighting factors: Furthermore, to deal with the potential filtering divergence of the algorithm and the position lost of the UAV, two additional weighting factors α and β, and the recorded offline matrices $\boldsymbol{R}_{offline}$ and $\boldsymbol{Q}_{offline}$ are introduced in the proposed algorithm. The offline data for these noise covariance matrices are estimated through the recorded multi-rounds sensor data with UAV statically at the original point before its flight. As the sensor data volume is directly relevant to the estimation accuracy and stability for the offline noise covariance matrices, thus, the number of the estimation rounds for this process should be carefully decided. With more estimation rounds, the initialization time for the positioning system will be increased, which may have the influence on the application scenarios of the system. Otherwise, the accidental errors may have the great impact on the accuracy of the offline noise covariance matrices. Therefore, in order to avoid all these problems, multi-round simulations and experiments have been conducted, and finally the 50 rounds is selected for this system which can achieve the less initialization time with an acceptable accuracy of the offline noise covariance matrices.

Firstly, the $\boldsymbol{R}$ matrix estimation is considered. Throughout α and $\boldsymbol{R}_{offline}$, the limited measurement noise covariance matrix $\boldsymbol{R}^*$ in the current round can be derived as

$$\boldsymbol{R}_k^* = (1-\alpha)\boldsymbol{R}_{offline} + \alpha \boldsymbol{R}_k. \tag{30}$$

Similarly, the limited process noise covariance matrix $\boldsymbol{Q}^*$ can be calculated by β and $\boldsymbol{Q}_{offline}$,

$$\boldsymbol{Q}_{k-1}^* = (1-\beta)\boldsymbol{Q}_{offline} + \beta \boldsymbol{Q}_{k-1}. \tag{31}$$

Obviously from (30) and (31), with the reduction of the weighting factors, the calculation for the limited noise covariance matrices will more rely on the offline data estimated during the offline phase. It means that the estimation results will become relatively stable and smooth. The probability for the filtering divergence or position lost can be decreased. Nevertheless, this will cause the adaptive ability loss. On the contrary, with the augment of the weighting factors, more changes for the estimation of these matrices will be brought in to catch up the variation of the process and measurement noise in the current round. This means that the localisation accuracy of the algorithm can be increased. Yet, its stability will be influenced and may even cause the filtering divergence and position loss. Clearly, the value of the additional weighting factors greatly influences the performance and stability of the proposed algorithm.

In order to find the suitable weighting factors, an adaptive estimation approach for these weighting factors is presented and given as follows. In the estimation process, α is utilised to limit the variation of the estimated measurement noise covariance matrix. It means that α has the relationship with the measurement noise in the current round. Therefore, the following equation is given to help for its estimation

$$\alpha' = \frac{\frac{1}{n}\sum_{i=1}^{n}[\boldsymbol{Z}_k'']_{i1}}{Z_{in}''}\alpha_{in}, \tag{32}$$

where, n is supposed to be the amount of the fixed anchor nodes, Z_{in}'' denotes the calculated and recorded innovation sequence in the offline phase and α_{in} is the initial value of α, which is set to be 0.2. The adaptively estimated α' is set within [0,0.2]. All these parameters are selected under the consideration of the stability of the algorithm. The principle for selecting the initial value of α and the range of α' is provided in Section IV-A.

Apparently from (32), along with increasing the innovation sequence $\boldsymbol{Z}_k''$, which means larger difference between the predicted measurements and the observation information in the current round, the α' will become larger. Otherwise, the α' will become smaller to keep the stable and smooth estimation of the measurement noise covariance matrix.

Similarly, the estimation of the weighting factor β can also be set up, according to the relationship with the process noise. Considering the time interval ΔT between the two rounds acceleration measurements has the impact on the prediction process, where with the larger ΔT, the influence of the process noise on the prediction process will become larger, otherwise, the influence can be reduced. Thus, the relationship between the time interval in the current round and the average time interval ΔT_{avg} calculated in the offline phase is utilised to estimate β. The calculation equation can be derived as follows

$$\beta' = \frac{\Delta T}{\Delta T_{avg}}\beta_{in}, \tag{33}$$

where, $\beta_{in} = 0.2$ is the initial value of the weighting factor, the range of the β' is set within [0,0.2]. Similarly, these values are selected under the consideration of the stability of the algorithm, and the principle for selecting the initial value and the determination for the range of β' is given in Section IV-A.

Apparently, with a larger ΔT which exceeds the ΔT_{avg}, the process noise will have more impact on the prediction performance. Thus, a larger β' will be estimated to give more trust to the current estimation results. On the contrary, a smaller ΔT means a smaller impact for the process noise on the prediction performance. Therefore, a smaller β' will be provided to keep a stable estimation. Finally, the structure of the proposed ASRCKF algorithm is provided in Fig.2 to give a clear view about it in comparison with the traditional SRCKF algorithm.

3) Computational complexity analysis: In addition to the accuracy and precision of the algorithm, the computational complexity also has the huge impact on its performance, especially for the UAV positioning algorithm. For computational complexity analysis, the floating point operations (flops) and big O notation will be applied. Firstly, for the calculation of the $\boldsymbol{\gamma}_{i,k-1}$, clearly, m flops will be required. Then for the propagated cubature points $\boldsymbol{\gamma}_{i,k/k-1}^*$, the value of flops will be $2m^2 - m$. Accordingly, the value of flops for the predicted state vector $\hat{\boldsymbol{\gamma}}_{k/k-1}$ and the square root of the covariance matrix $\boldsymbol{S}_{k/k-1}$ will be $2m^2$ and $8m^3+4m^2+2m$,

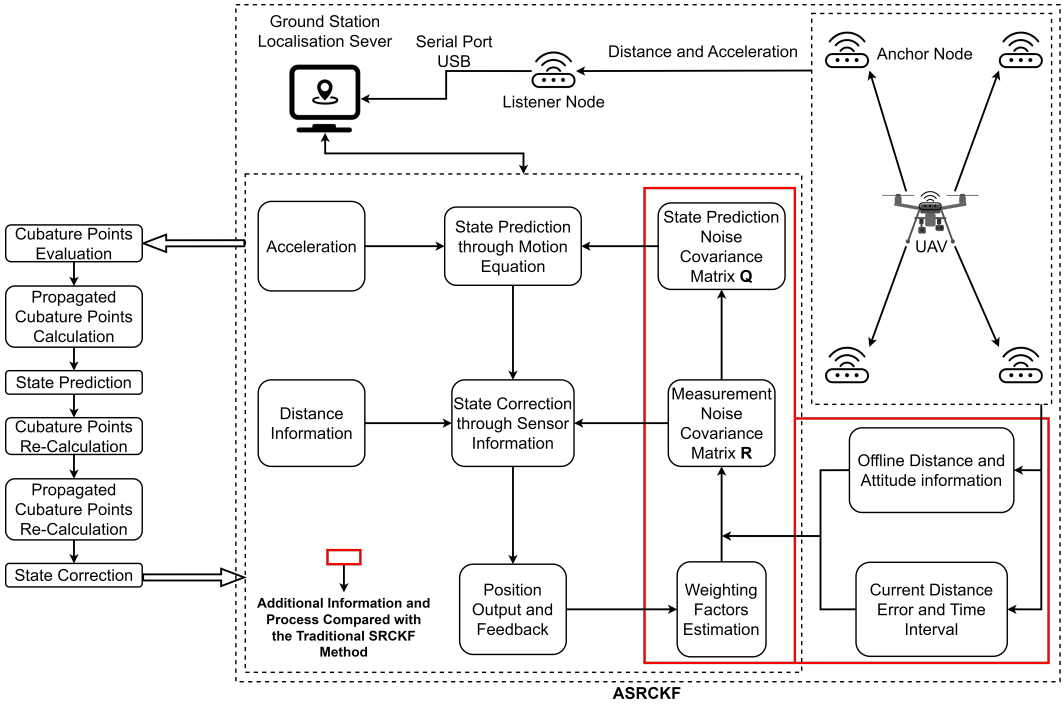

Fig. 2. Algorithm structure.

respectively. Then for the correction process, the value of flops for the cubature points $\boldsymbol{\gamma}_{i,k/k-1}$ is m. The flops for the propagated cubature points $\boldsymbol{Z}_{i,k/k-1}$ and the predicted measurement matrix $\hat{\boldsymbol{Z}}_{k/k-1}$ in correction process will be $2mn - n$ and $2mn$, respectively. Then, the flops value for the Kalman gain $\boldsymbol{K}_{k,gain}$, corrected state vector $\hat{\boldsymbol{\gamma}}_k$ and the square root of the covariance matrix $\hat{\boldsymbol{S}}_k$ can be known as $2n^3 + 4mn^2 - 2mn$, $2mn + n$ and $8m^3 + 4m^2 + 2m$, respectively. Finally, for the noise model estimation process, through the calculation process, it can be known that the flops value for the $\boldsymbol{R}$ matrix, $\boldsymbol{Q}$ matrix and weighting factors are all below n^3. In conclusion, with all the flops for the variables within the algorithm, it can be obtained that the computational complexity for the proposed ASRCKF algorithm is within $O(m^3)$ and $O(n^3)$ level.

IV. Simulation and Experiment

For the purpose of providing the comprehensive and quantitative validation of the proposed ASRCKF localisation algorithm and the UAV system, the simulations in the Gazebo environment [41] and the experiments in laboratory environment have been conducted.

A. Simulation

Under the consideration of the safety reason for the actual flight tests, the simulations for the proposed localisation algorithm on the UAV have been conducted. In order to mock the actual focused application scenarios and verify the performance of the presented algorithm, the operational space is set as 1.95 $\times$ 3.0 $\times$ 2.3 (m) with no GPS signals avaiable. The entrance of the working space for the UAV is supposed on the X-Z plane. It needs to declare that even the performance of the algorithm and the system can be improved with more anchor nodes or with the geometry configuration of the anchor nodes can cover the whole localisation area, however, as aforementioned, for the focused applications in this paper, it is difficult for the engineer to get into such space to deploy the anchor nodes. Therefore, in order to mock the situation that there is no requirement for the engineer to get into the space to deploy the fixed anchor nodes, all the anchor nodes are disposed on the X-Z plane near the entrance. The detailed X, Y, Z coordinates of all the anchor nodes are given in Table I.

The UAV flight path in the simulation is set as a reverse "S", which is to provide a more comprehensive evaluation for the performance of the proposed algorithm. The STD for the measurement noise is supposed to be a randomly changing value from 0m to 0.2m, which is to mock the changing measurement noise caused by the communication condition variation between the sensor nodes in actual environment. In the simulation, six algorithms including the pure UWB based localisation algorithm, EKF, SRCKF, ASRCKF with constant weighting factors and the AEKF proposed in our previous work [38] have been tested and compared to comprehensively verify the effectiveness of the proposed algorithm before the actual flight tests. The simulation results, e.g. the flight trajectories of each algorithm, the flight trajectories in X, Y, Z directions, the ground truth for the flight trajectories of each algorithm, the ground truth for the flight trajectories in X, Y, Z directions, the root mean square error (RMSE) of each algorithm in X, Y, Z directions and the empirical cumulative distribution function (eCDF) of each have been depicted in Fig. 3. Furthermore, in order to provide a clear

TABLE I
COORDINATES OF THE ANCHOR NODES.

Coordinates	Fixed Anchor Node 1	Fixed Anchor Node 2	Fixed Anchor Node 3	Fixed Anchor Node 4
X	0.00m	1.95m	0.00m	1.95m
Y	0.00m	0.00m	0.00m	0.00m
Z	0.00m	0.00m	2.30m	2.30m

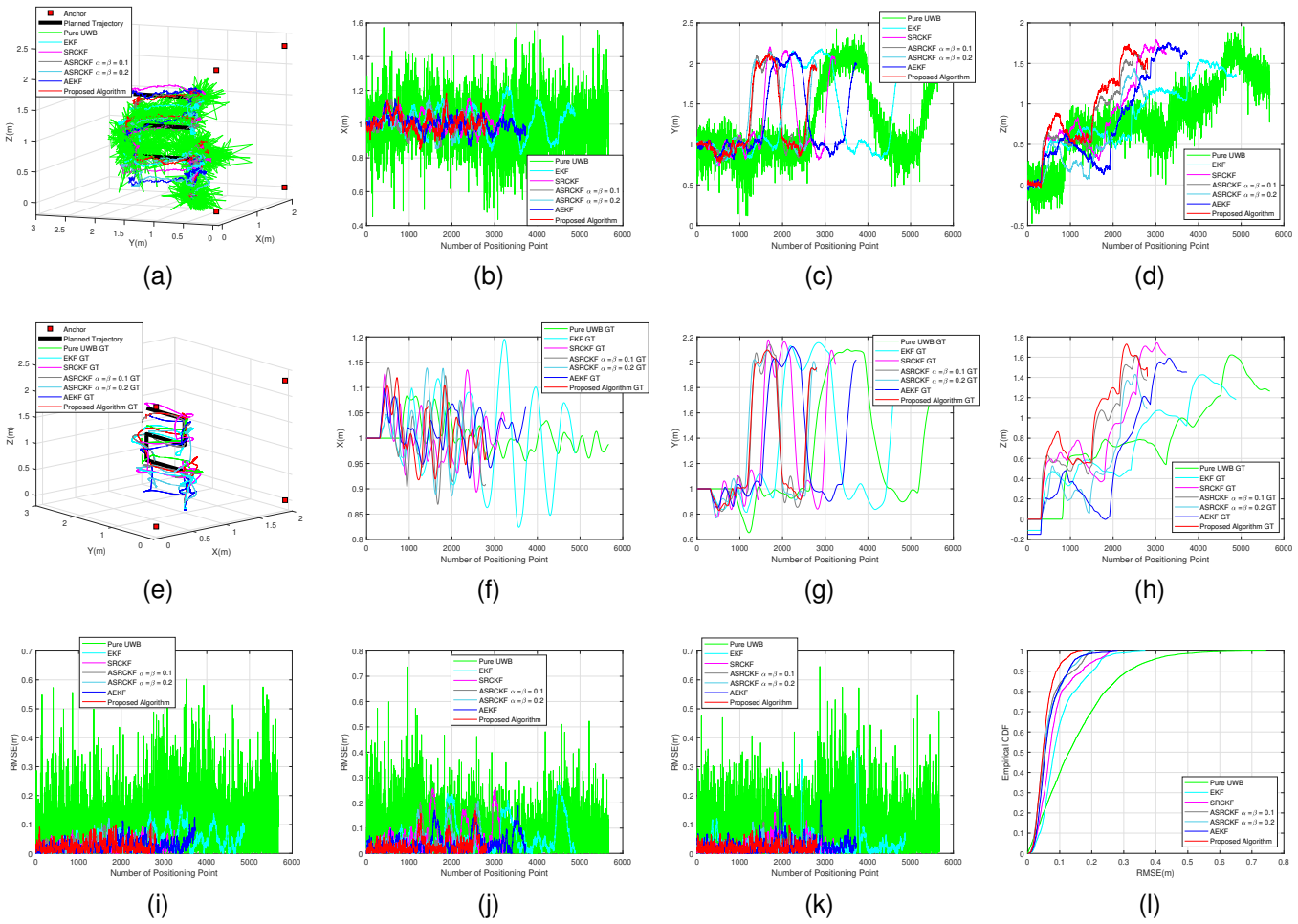

Fig. 3. Flight test results in the simulation environment. (a) UAV 3D trajectories in the simulation. (b) X direction trajectories for the UAV. (c) Y direction trajectories for the UAV. (d) Z direction trajectories for the UAV. (e) Ground truth for UAV 3D trajectories in the simulation. (f) Ground truth for X direction trajectories. (g) Ground truth for Y direction trajectories. (h) Ground truth for Z direction trajectories. (i) X direction RMSE (m) calculated through ground truth. (j) Y direction RMSE (k) calculated through ground truth. (l) RMSE (m) in Z direction calculated through ground truth. (m) eCDF.

view for the performance of each algorithm, the detailed performance information including the median localisation error, 95^{th} percentile localisation error and the average STD of the RMSE has also been provided in Table II.

Obviously, the pure UWB based localisation algorithm has the worst localisation performance due to the large measurement noise and the unreasonable value within the ranging information. With the integration of the IMU for the sensor fusion approaches such as the EKF, this performance influence is greatly reduced with 0.082m median localisation error, 0.227m 95^{th} percentile localisation error and 0.063m average STD. However, the localisation performance is still limited by the neglected high order terms within the observation matrix and the unknown noise covariance matrices. To overcome these, leveraging the cubature rule, the state posterior mean and covariance can be approximated by the SRCKF for performance improvement, which successfully reduced the median localisation error, 95^{th} percentile localisation error and average STD to 0.069m, 0.208m and 0.054m. Nevertheless, the SRCKF is still suffer from the performance influence led by the unknown noise covariance matrices. To remedy this, the adaptive sensor fusion based approach can be an ideal candidate. Here, two different adaptive sensor fusion approaches including the ASRCKF with constant weighting factors and the AEKF with the estimated weighting factors in [38] are tested and compared with the proposed algorithm. Obviously, with the estimated noise covariance matrices for these adaptive sensor fusion based approaches, the localisation

TABLE II
DETAILED SIMULATION RESULTS

	Median Error	Improved	95^{th} Percentile Error	Improved	Average STD	Improved
Pure UWB based localisation algorithm	0.129m	N/A	0.380m	N/A	0.116m	N/A
EKF	0.082m	36.4%	0.227m	40.2%	0.063m	45.7%
SRCKF	0.069m	46.5%	0.208m	45.3%	0.054m	53.4%
ASRCKF ($\alpha = \beta = 0.1$)	0.052m	59.7%	0.173m	54.5%	0.045m	61.2%
ASRCKF ($\alpha = \beta = 0.2$)	0.050m	61.2%	0.160m	57.9%	0.042m	63.8%
AEKF [38]	0.055m	57.4%	0.144m	62.1%	0.041m	64.7%
Proposed algorithm	**0.047m**	**63.6%**	**0.110m**	**71.1%**	**0.028m**	**75.9%**

performance is significantly improved with the median localisation error around 0.05m, the 95^{th} percentile localisation error around 0.160m and the average STD around 0.040m. Especially for the proposed algorithm, with the ability to deal with the linearisation issue for the observation matrix, the adaptively estimated noise model and the estimated weighting factors, the best performance can be obtained by the proposed algorithm with the median localisation error, 95^{th} percentile localisation error and average STD to be 0.047m, 0.110m and 0.028m, respectively. Compared with the pure UWB based localisation algorithm, these three indexes are improved 63.6%, 71.1% and 75.9%, respectively. However, it still needs to declare that only the smaller constant weighting factors (0.1 and 0.2) selected here is under the consideration for the stability of the algorithm. Larger weighting factors means the estimation results for the noise covariance matrices will more rely on the current estimation results, which will lead to more variations of the noise covariance matrices and may cause the filtering divergence. According to the simulation results, with the ASRCKF algorithm, when the weighting factors exceed 0.5, the probability for filtering divergence will be increased significantly. Even with the relatively smaller weighting factors (0.3 or 0.4), the filtering divergence still exists under certain circumstances. Since the primary objective for the UAV localisation system in dark and GPS-denied environment is to prevent any positioning failure, the relatively smaller weighting factors (0.1 and 0.2) are selected, the estimation results for the weighting factors of the proposed algorithm are limited within [0,0.2] and the initial value of these are set as 0.2.

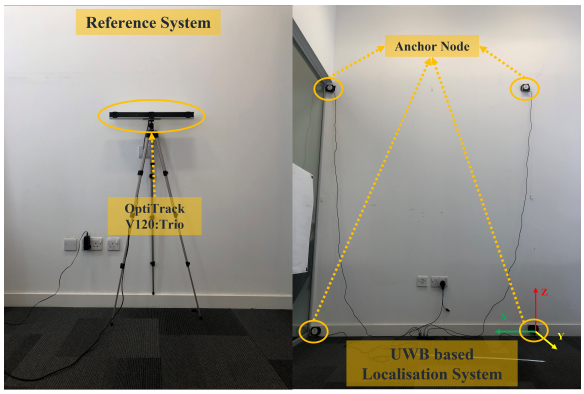

Fig. 4. Experiment environment.

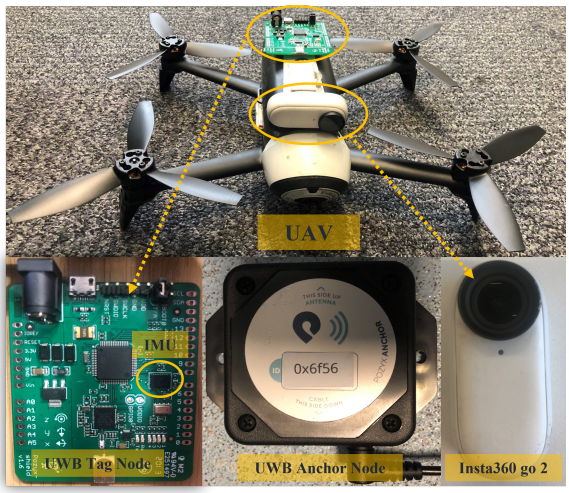

Fig. 5. System components.

B. Experiment

1) Experiment configuration: For the purpose of further evaluating the performance of the proposed algorithm and UAV positioning system, the actual experiments in the laboratory environment have been conducted. Similarly, the localisation area for the actual experiments has the same size as in the simulation environment 1.95 × 3.0 × 2.3 (m), and the GPS is unavailable in such environment, in order to comprehensively verify the effectiveness of the proposed system and algorithm. The geometry configuration for the anchor nodes is also kept as the same. The clear view about the laboratory experiment environment, geometry configuration of the anchor nodes and the components utilised in the system are shown in Fig. 4 and Fig. 5.

2) Performance evaluation and comparison: In the performance evaluation and comparison experiments, the markers are attached on the UAV to help the reference system to get the sub-millimeter accuracy position information for the UAV to provide the ground truth. The planned path for the UAV in the experiments is the same as it in the simulations. All the algorithms including the pure UWB, EKF, SRCKF, ASRCKF with constant weighting factors (α and β equal to 0.1 and 0.2), the AEKF proposed in our previous work [38] and the proposed algorithm have been tested and evaluated. The trajectories, ground truth, RMSE results and the detailed localisation error for each algorithm have been given in Fig.

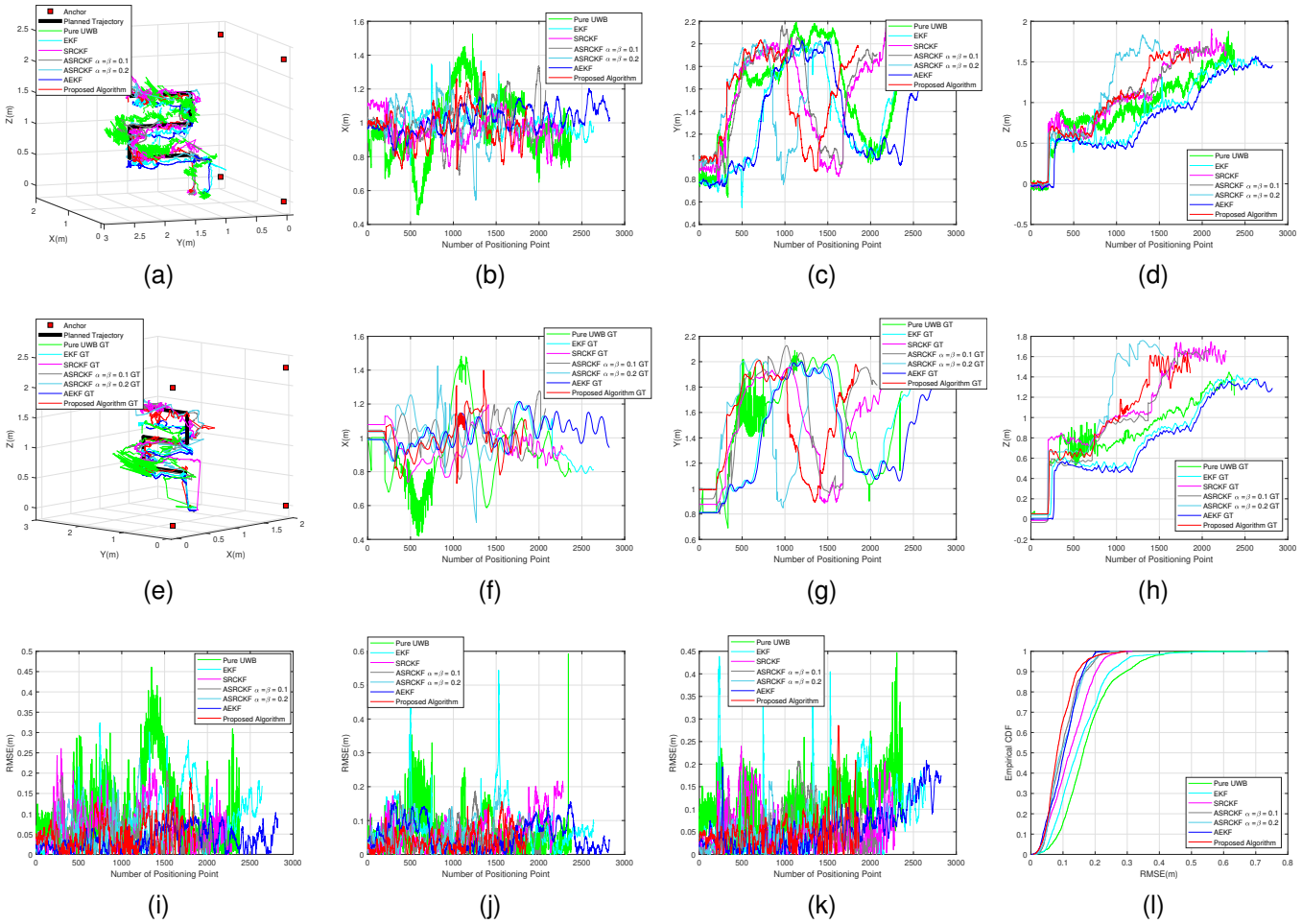

Fig. 6. Flight test results of performance evaluation tests. (a) UAV 3D trajectories in the performance evaluation tests. (b) X direction trajectories for the UAV. (c) Y direction trajectories for the UAV. (d) Z direction trajectories for the UAV. (e) Ground truth for UAV 3D trajectories in the performance evaluation tests. (f) Ground truth for X direction trajectories. (g) Ground truth for Y direction trajectories. (h) Ground truth for Z direction trajectories. (i) X direction RMSE (m) calculated through ground truth. (j) Y direction RMSE (m) calculated through ground truth. (k) RMSE (m) in Z direction calculated through ground truth. (l) eCDF.

TABLE III
DETAILED EXPERIMENT RESULTS

	Median Error	Improved	95^{th} Percentile Error	Improved	Average STD	Improved	Update Rate
Pure UWB based localisation algorithm	0.163m	N/A	0.342m	N/A	0.083m	N/A	25Hz
EKF	0.143m	12.3%	0.287m	16.1%	0.080m	3.6%	**90Hz**
SRCKF	0.121m	25.8%	0.223m	34.8%	0.060m	27.7%	70Hz
ASRCKF ($\alpha = \beta = 0.1$)	0.095m	41.7%	0.198m	42.1%	0.048m	42.2%	68Hz
ASRCKF ($\alpha = \beta = 0.2$)	0.092m	43.6%	0.194m	43.3%	0.049m	41.0%	68Hz
AEKF [38]	0.102m	37.4%	0.176m	48.5%	0.046m	44.6%	88Hz
Proposed algorithm	**0.081m**	**50.3%**	**0.172m**	**49.7%**	**0.045m**	**45.8%**	66Hz

6 and Table III.

Throughout the analysis of the RMSE results in Fig. 6, it can be known that the largest performance oscillation can be found for the pure UWB based algorithm, which is caused by the unreasonable value and the measurement noise within the observation information from the UWB sensor nodes. This phenomenon can also be shown by the detailed localisation results in Table III, where the worst localisation performance with 0.163m median localisation error, 0.342m 95^{th} percentile localisation error and 0.083m average STD was recorded for the pure UWB based localisation algorithm. With the introduction of the additional IMU, this performance degradation led by the unreasonable value and the measurement noise can be limited. Clearly, for all the IMU and UWB based sensor fusion approaches, the median localisation error, 95^{th} percentile localisation error and average STD are all limited within 0.15m, 0.29m and 0.08m, respectively. However, same as the simulations, the performance influence still exists for the EKF, due to the linearisation of the observation matrix and the unsuitable noise covariance matrices. Even, this influence can

be successfully eliminated by the SRCKF with the cubature rule which attained the 0.121m median localisation error, 0.223m 95^{th} percentile localisation error and 0.06m average STD. Yet, the influence from the unsuitable noise covariance matrices exists as before.

To further improve the localisation performance of the system under such circumstance, the AKF based methods can be an ideal candidate. Leveraging the adaptive ability of the AEKF in [38], ASRCKF with constant weighting factors and the proposed algorithm, the $\boldsymbol{Q}$ and $\boldsymbol{R}$ matrices can be adaptively estimated to catch up the changes for the process and measurement noise within the system. According to the experiment results, the localisation performance for the system can be significantly improved with the median localisation error, 95^{th} percentile localisation error and average STD around 0.1m, 0.18m and 0.047m, when in comparison with the EKF and SRCKF with constant and manually adjusted noise covariance matrices. Then, for the comparison within the adaptive approaches. When with the ability to deal with the influence from the linearisation of the observation matrix, and the adaptively estimated weighting factors to limit the estimation of the noise covariance matrices to get rid of any potential filtering divergence and eliminate the performance oscillation, the best performance can be obtained by the proposed algorithm. It can be observed that the proposed algorithm can attain 0.081m median localisation error, 0.172m 95^{th} percentile localisation error and 0.045m average STD.

On the other hand, in addition to the localisation accuracy and precision, the position update rate for the algorithm also has a close link with the stability of the UAV in our focused environments. The update rate for the position information is directly related to the complexity of the algorithm when it is with the same measurement frequency of IMU and UWB sensors. Clearly from Table III, the pure UWB based localisation algorithm can only achieve the 25Hz update rate, due to the ranging frequency of the UWB. The EKF based algorithm which has the lowest complexity can attain 90Hz position update rate with the participation of the IMU measurements. For the proposed algorithm, even it can only obtain the 66Hz position update rate with the highest algorithm complexity, however, it is only a slight increase compared with the AEKF algorithm in our previous work. Furthermore, considering the response speed of the UAV controller, the 66Hz update rate is already enough for the UAV to maintain its stability in focused environments. Therefore, even the algorithm complexity of the proposed algorithm is slightly increased, nevertheless, with the highest positioning performance, it is still the best option for the UAV localisation in the focused environments.

3) Actual application in laboratory environment: Considering the focused applications are the autonomous inspection inside dark and GPS-denied environments. Thus, in order to comprehensively verify the practicality for focused applications, the detailed inspection experiment has been carried out. The inspection area is set the same as in the experiment flight test. For this flight test, the purpose is to verify inspection ability of the designed system and the algorithm. Therefore, different from the previous experiments, the path of the UAV is calculated to cover the entire localisation area for detailed inspection. The video for this flight test can be found in the link [1]. The UAV trajectories for the test have been given and depicted in Fig. 7. Due to the complexity of the calculated path, the measured position information from the current reference system may be significantly influenced as only three cameras are available for the motion capture. Therefore, the ground truth for this test is not provided.

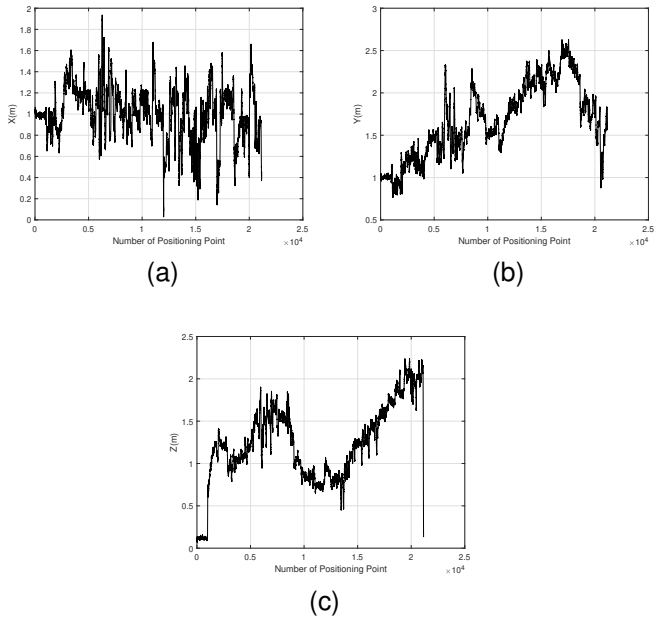

Fig. 7. Flight trajectory for ASRCKF based autonomous inspection. (a) Trajectory in X(m) direction in the autonomous inspection flight test. (b) Trajectory in Y(m) direction in the autonomous inspection flight test. (c) Trajectory in Z(m) direction in the autonomous inspection flight test.

V. Conclusion

In this article, an ASRCKF based UAV positioning algorithm and a low cost UAV positioning system have been proposed and designed to achieve the detailed UAV assisted inspection inside dark and GPS-denied environments to substitute humans. At the beginning, the review on the existing UAV localisation techniques was conducted to identify the potential issues and requirements for inspection applications inside such environment. Then, the detailed description for the system diagram was made to give the clear view about the designed system and its main characteristics. Afterwards, the introduction for the proposed ASRCKF based UAV positioning algorithm was given. Due to the drawbacks of UWB techniques and the traditional KF algorithms, such as the performance influence caused by the measurement noise variation and unreasonable values for the observation information, the linearisation of the observation matrix, the unknown noise model and the potential negative estimation for these noise matrices, the ASRCKF based algorithm was proposed. Leveraging the integration with IMU, the cubature rule, the adaptively estimated noise model and weighting factors, all the aforementioned issues can be solved for reliable, high precision and accuracy UAV

[1] https://youtu.be/KNKibl3Lqog

localisation in dark and GPS-denied environments. Finally, numerical simulations and experiments were conducted to evaluate the performance and validate the effectiveness of the proposed system and algorithm. Evidenced from the simulation and experiment results, the presented algorithm in this paper is able to resolve the aforementioned problems and attain high accuracy and precision positioning performance, which is capable for the detailed autonomous inspection in such environment to substitute humans. For further confirmation, the autonomous inspection experiment was also conducted. In summary, the proposed algorithm and system are able to achieve the low cost UAV autonomous inspection in dark and GPS-denied environments.

REFERENCES

[1] F. Bonnin-Pascual, A. Ortiz, E. Garcia-Fidalgo, and J. P. Company-Corcoles, "A reconfigurable framework to turn a mav into an effective tool for vessel inspection," *Robot. Comput. Integr. Manuf.*, vol. 56, pp. 191–211, 2019.

[2] B. Yang, E. Yang, L. Yu, and C. Niu, "Ultrasonic- and imu-based high-precision uav localization for the low-cost autonomous inspection in oil and gas pressure vessels," *IEEE Trans. Ind. Informat.*, vol. 19, no. 10, pp. 10 523–10 534, 2023.

[3] J. Li, H. Shi, and K.-S. Hwang, "Using goal-conditioned reinforcement learning with deep imitation to control robot arm in flexible flat cable assembly task," *IEEE Trans. Autom. Sci. Eng.*, pp. 1–12, 2023.

[4] Y. Xue and W. Chen, "Multi-agent deep reinforcement learning for uavs navigation in unknown complex environment," *IEEE Trans. Intell. Veh.*, early access,2023, doi: 10.1109/TIV.2023.3298292.

[5] L. Yang, J. Fan, Y. Liu, E. Li, J. Peng, and Z. Liang, "A review on state-of-the-art power line inspection techniques," *IEEE Trans. Instrum. Meas.*, vol. 69, no. 12, pp. 9350–9365, 2020.

[6] Z. He, J. Li, F. Wu, H. Shi, and K.-S. Hwang, "Derl: Coupling decomposition in action space for reinforcement learning task," *IEEE Trans. Emerg. Topics Comput. Intell.*, vol. 8, no. 1, pp. 1030–1043, 2024.

[7] J. Li, H. Shi, H. Wu, C. Zhao, and K.-S. Hwang, "Eliminating primacy bias in online reinforcement learning by self-distillation," *IEEE Trans. Neural Netw.*, pp. 1–13, 2024.

[8] J. Chen, N. Zhao, R. Zhang, L. Chen, K. Huang, and Z. Qiu, "Refined crack detection via lecsformer for autonomous road inspection vehicles," *IEEE Trans. Intell. Veh.*, vol. 8, no. 3, pp. 2049–2061, 2023.

[9] L. Fan, D. Wang, J. Wang, Y. Li, Y. Cao, Y. Liu, X. Chen, and Y. Wang, "Pavement defect detection with deep learning: A comprehensive survey," *IEEE Trans. Intell. Veh.*, vol. 9, no. 3, pp. 4292–4311, 2024.

[10] B. Yang and E. Yang, "A survey on radio frequency based precise localisation technology for uav in gps-denied environment," *J. Intell. Robot. Syst.*, vol. 103, no. 3, pp. 1–30, 2021.

[11] Y. Gao, H. Jing, M. Dianati, C. M. Hancock, and X. Meng, "Performance analysis of robust cooperative positioning based on gps/uwb integration for connected autonomous vehicles," *IEEE Trans. Intell. Veh.*, vol. 8, no. 1, pp. 790–802, 2023.

[12] Y. Zou, E. Hu, Z. Deng, and C. Jin, "Multidimensional scaling algorithm for mobile swarming uavs localization," *IEEE Trans. Intell. Veh.*, early access,2023, doi: 10.1109/TIV.2023.3325806.

[13] S. Teng, L. Li, Y. Li, X. Hu, L. Li, Y. Ai, and L. Chen, "Fusionplanner: A multi-task motion planner for mining trucks via multi-sensor fusion," *Mech. Syst. Signal Process.*, vol. 208, p. 111051, 2024. [Online]. Available: https://www.sciencedirect.com/science/article/pii/S0888327023009597

[14] H. Shi, L. Shi, M. Xu, and K.-S. Hwang, "End-to-end navigation strategy with deep reinforcement learning for mobile robots," *IEEE Trans. Ind. Informat.*, vol. 16, no. 4, pp. 2393–2402, 2020.

[15] H. Wei, H. Zhang, A.-H. Kamal, and Y. Shi, "Ensuring secure platooning of constrained intelligent and connected vehicles against byzantine attacks: A distributed mpc framework," *Engineering*, vol. 33, pp. 35–46, 2024.

[16] L. Yu, E. Yang, B. Yang, Z. Fei, and C. Niu, "A robust learned feature-based visual odometry system for uav pose estimation in challenging indoor environments," *IEEE Trans. Instrum. Meas.*, vol. 72, pp. 1–11, 2023.

[17] H. Wei, B. Lou, Z. Zhang, B. Liang, F.-Y. Wang, and C. Lv, "Autonomous navigation for evtol: Review and future perspectives," *IEEE Trans. Intell. Veh.*, 2024.

[18] C. Kanellakis, P. S. Karvelis, S. S. Mansouri, A.-A. Agha-Mohammadi, and G. Nikolakopoulos, "Towards autonomous aerial scouting using multi-rotors in subterranean tunnel navigation," *IEEE Access*, vol. 9, pp. 66 477–66 485, 2021.

[19] Z. Wang, S. Liu, G. Chen, and W. Dong, "Robust visual positioning of the uav for the under bridge inspection with a ground guided vehicle," *IEEE Trans. Instrum. Meas.*, vol. 71, pp. 1–10, 2021.

[20] P. Tripicchio, M. Satler, M. Unetti, and C. A. Avizzano, "Confined spaces industrial inspection with micro aerial vehicles and laser range finder localization," *Int. J. Micro Air Vehicles*, vol. 10, no. 2, pp. 207–224, 2018.

[21] T. Özaslan, G. Loianno, J. Keller, C. J. Taylor, and V. Kumar, "Spatio-temporally smooth local mapping and state estimation inside generalized cylinders with micro aerial vehicles," *IEEE Robot. Autom. Lett.*, vol. 3, no. 4, pp. 4209–4216, 2018.

[22] M. Petrlík, T. Báča, D. Heřt, M. Vrba, T. Krajník, and M. Saska, "A robust uav system for operations in a constrained environment," *IEEE Robot. Autom. Lett.*, vol. 5, no. 2, pp. 2169–2176, 2020.

[23] P. Petráček, V. Krátkỳ, and M. Saska, "Dronument: System for reliable deployment of micro aerial vehicles in dark areas of large historical monuments," *IEEE Robot. Autom. Lett.*, vol. 5, no. 2, pp. 2078–2085, 2020.

[24] D. Feng, C. Wang, C. He, Y. Zhuang, and X.-G. Xia, "Kalman-filter-based integration of imu and uwb for high-accuracy indoor positioning and navigation," *IEEE Internet Things J.*, vol. 7, no. 4, pp. 3133–3146, 2020.

[25] B. Yang, E. Yang, L. Yu, and A. Loeliger, "High-precision uwb-based localisation for uav in extremely confined environments," *IEEE Sensors J.*, vol. 22, no. 1, pp. 1020–1029, 2021.

[26] K. Guo, Z. Qiu, C. Miao, A. H. Zaini, C.-L. Chen, W. Meng, and L. Xie, "Ultra-wideband-based localization for quadcopter navigation," *Unmanned Syst.*, vol. 4, no. 01, pp. 23–34, 2016.

[27] J. Li, Y. Bi, K. Li, K. Wang, F. Lin, and B. M. Chen, "Accurate 3d localization for mav swarms by uwb and imu fusion," in *Proc. 14th IEEE Int. Conf. Control Automat.* IEEE, 2018, pp. 100–105.

[28] M. Strohmeier, T. Walter, J. Rothe, and S. Montenegro, "Ultra-wideband based pose estimation for small unmanned aerial vehicles," *IEEE Access*, vol. 6, pp. 57 526–57 535, 2018.

[29] W. You, F. Li, L. Liao, and M. Huang, "Data fusion of uwb and imu based on unscented kalman filter for indoor localization of quadrotor uav," *IEEE Access*, vol. 8, pp. 64 971–64 981, 2020.

[30] B. Gao, G. Hu, Y. Zhong, and X. Zhu, "Cubature kalman filter with both adaptability and robustness for tightly-coupled gnss/ins integration," *IEEE Sensors J.*, vol. 21, no. 13, pp. 14 997–15 011, 2021.

[31] I. Arasaratnam and S. Haykin, "Cubature kalman filters," *IEEE Trans. Autom. Control*, vol. 54, no. 6, pp. 1254–1269, 2009.

[32] C. Shen, Y. Zhang, X. Guo, X. Chen, H. Cao, J. Tang, J. Li, and J. Liu, "Seamless gps/inertial navigation system based on self-learning square-root cubature kalman filter," *IEEE Trans. Ind. Electron.*, vol. 68, no. 1, pp. 499–508, 2020.

[33] A. Mohamed and K. Schwarz, "Adaptive kalman filtering for ins/gps," *J. Geod.*, vol. 73, no. 4, pp. 193–203, 1999.

[34] M. Narasimhappa, A. D. Mahindrakar, V. C. Guizilini, M. H. Terra, and S. L. Sabat, "Mems-based imu drift minimization: Sage husa adaptive robust kalman filtering," *IEEE Sensors J.*, vol. 20, no. 1, pp. 250–260, 2019.

[35] M. Song, R. Astroza, H. Ebrahimian, B. Moaveni, and C. Papadimitriou, "Adaptive kalman filters for nonlinear finite element model updating," *Mech. Syst. Signal Process.*, vol. 143, p. 106837, 2020.

[36] Y. Huang, Y. Zhang, B. Xu, Z. Wu, and J. A. Chambers, "A new adaptive extended kalman filter for cooperative localization," *IEEE Trans. Aerosp. Electron. Syst.*, vol. 54, no. 1, pp. 353–368, 2017.

[37] Y. Huang, M. Bai, Y. Li, Y. Zhang, and J. Chambers, "An improved variational adaptive kalman filter for cooperative localization," *IEEE Sensors J.*, vol. 21, no. 9, pp. 10 775–10 786, 2021.

[38] B. Yang, E. Yang, L. Yu, and C. Niu, "Adaptive extended kalman filter-based fusion approach for high-precision uav positioning in extremely confined environments," *IEEE/ASME Trans. Mechatronics*, vol. 28, no. 1, pp. 543–554, 2023.

[39] A. Benini, A. Mancini, and S. Longhi, "An imu/uwb/vision-based extended kalman filter for mini-uav localization in indoor environment using 802.15. 4a wireless sensor network," *J. Intell. Robot. Syst.*, vol. 70, no. 1, pp. 461–476, 2013.

[40] S. Akhlaghi, N. Zhou, and Z. Huang, "Adaptive adjustment of noise covariance in kalman filter for dynamic state estimation," in *Proc. IEEE Power Energy Soc. Gen. Meeting*. IEEE, 2017, pp. 1–5.
[41] Gazebo. Gazebo online tutorial. [Online]. Available: https://gazebosim.org

Beiya Yang (Member, IEEE) received the B.Eng. degree in Electronic Information Engineering from Northwestern Polytechnical University, Xi'an, China, in 2013 and the M.Sc degree in Information and Communication Engineering from National University of Defense Technology, Changsha, China, in 2015. He received his Ph.D. degree in high-precision positioning technology, from the Department of Design, Manufacturing and Engineering Management (DMEM), University of Strathclyde, Glasgow, UK, in 2023. His current research interests include indoor localisation technology and wireless sensor networks.

Erfu Yang (Senior Member, IEEE) received his Ph.D. degree in Robotics from the School of Computer Science and Electronic Engineering, University of Essex, Colchester, UK, in 2008. He is currently a Senior Lecturer in the Department of Design, Manufacturing and Engineering Management (DMEM), University of Strathclyde, Glasgow, UK. His main research interests include robotics, autonomous systems, mechatronics, manufacturing automation, signal and image processing, computer vision and applications of machine learning and artificial intelligence, etc. He has over 180 publications in these areas, including more than 80 journal papers and 10 book chapters. Dr. Yang has been awarded over 15 research grants as PI (principal investigator) or CI (co-investigator). He is the Fellow of the UK Higher Education Academy, Member of the UK Engineering Professors' Council, Senior Member of the IEEE Society of Robotics and Automation, IEEE Control Systems Society, Publicity Co-Chair of the IEEE UK and Ireland Industry Applications Chapter, Committee Member of the IET SCOTLAND Manufacturing Technical Network. He is also an associate editor for the Cognitive Computation journal published by Springer.

Haobin Shi Haobin Shi received the Ph.D. degree in computer science and technology from Northwestern Polytechnical University, Xi'an, China, in 2008. He is currently a Professor with the School of Computer Science, Northwestern Polytechnical University, and Visiting Scholar of Electrical Engineering Department, National Sun Yat-sen University, Kaohsiung City, Taiwan. He is the Director of the Chinese Association for Artificial Intelligence. His research interests include intelligent robots, decision support systems, artificial intelligence, multi-agent systems, and machine learning.

Leijian Yu (Member, IEEE) received the B.Eng. degree in electrical information engineering and the M.Sc degree in information and communication engineering from China University of Petroleum (East China), Qingdao, China, in 2015 and 2018, respectively. He received his Ph.D. degree in robotics and autonomous systems for asset visual inspection, with the Department of Design, Manufacturing and Engineering Management (DMEM) at the University of Strathclyde, Glasgow, UK, in December 2023. His current research interests include machine learning, vision-based autonomous navigation and image contrast enhancement.

Cong Niu (Member, IEEE) has been awarded the B.Eng. with Honours, degree of Electronic Engineering from University of Central Lancashire, Preston, UK in 2014. Then awarded with the M.Sc degree on Embedded Digital System from University of Sussex, Brighton, UK in 2015. He received his Ph.D. degree in robotics and autonomous systems for agriculture applications, from the Department of Design, Manufacturing and Engineering Management (DMEM), University of Strathclyde, Glasgow, UK, in 2021. His current research interests include field and indoor path planning, modeling and simulation, unmanned ground and aerial vehicles and smart factory.